Multiconnected Interleaved Boost Converter for Hybrid Energy System

Sree Lakshmi Vineetha Bitragunta
Bitraguntavineetha@gmail.com

Abstract **- Concern over the condition of our decaying planet is making environmentally friendly solutions more popular than before. A novel front-end rectifier stage layout for a hybrid solar/fuel system is presented in this research. Depending on the energy sources' availability, this arrangement enables the two sources to serve the load either independently or concurrently. This interleaved boost converter's intrinsic feature is that it can filter out high frequency harmonics without the need for extra input filters. The longevity, heating problems, and efficiency of the converter are all negatively impacted by harmonic content. Additionally, Maximum Power Point Tracking (MPPT) enables the fused multi-input rectifier stage to maximize solar power when it is available. For the PV system, the conventional perturb and observe approach will be applied. To demonstrate the advantages of the suggested circuit, simulation results are provided. This technique can be used for both online and offline applications.**

I. INTRODUCTION

Due to growing concerns about global warming and the depletion of fossil fuel supplies, many people are looking for sustainable energy alternatives to save the world for future generations. With hydropower being the exception, wind and solar energy have the most potential to supply our energy needs[1]. Even though the sun is always there, the amount of solar irradiation changes according on the power of the light and the unpredictable shadows cast by clouds, trees, birds, and other objects. Photovoltaic systems' unreliability stemming from their intermittent nature is one of their main inherent drawbacks. When these two intermittent sources are combined and maximum power point tracking (MPPT) algorithms are used, however, the system's power transfer efficiency and reliability can be significantly improved[2,3].

Since people are worried about the depletion of fossil fuels and the environmental issues brought on by traditional power generation, renewable energy sources—such as fuel cells and photovoltaic (PV) panels—are becoming more and more popular. Batteries, water pumps, household power supplies, swimming pool heating systems, satellite power systems, and more are just a few of the various uses for photovoltaic sources nowadays. They are less polluting and require less maintenance, but in most cases, they are expensive to install. For the load interface, they need an interleaved boost converter (power converter). In recent years, production costs have decreased for wider use thanks to advancements in technology and production.

One module's power output is rarely sufficient to suit a home's needs. The other energy source can make up the difference when one is unavailable or cannot adequately supply the demands of the load[4].

There have been several hybrid PV/fuel power systems proposed [5-7]and investigated that are MPPT-controlled. A separate DC/DC interleaved boost converter coupled in parallel at the rectifier stage is used by most systems in the literature to achieve MPPT control for each renewable energy power source, as shown in Figure 1. A more simple multi-input structure that combines the sources from the DC-end has been developed to accomplish MPPT for each renewable source. The hybrid energy system and interleaved boost converter are combined in the proposed design.

For hybrid solar/fuel energy systems, a different multi-input rectifier structure is suggested in this research. The proposed topology has the following characteristics: 1) it does not require separate input filters due to the inherent nature of these converters; 2)

it can support step up/down operations for each renewable source (supporting a wide range of PV and fuel input); 3) MPPT can be realized for the source; and 4) it supports both individual and simultaneous operation. Results from simulations are shown to confirm that the suggested system is feasible[8].

II. PROPOSED METHODODLOGY

The main objective is to create, model, and deploy a multi-connected interleaved boost converter hybrid solar/fuel cell system.

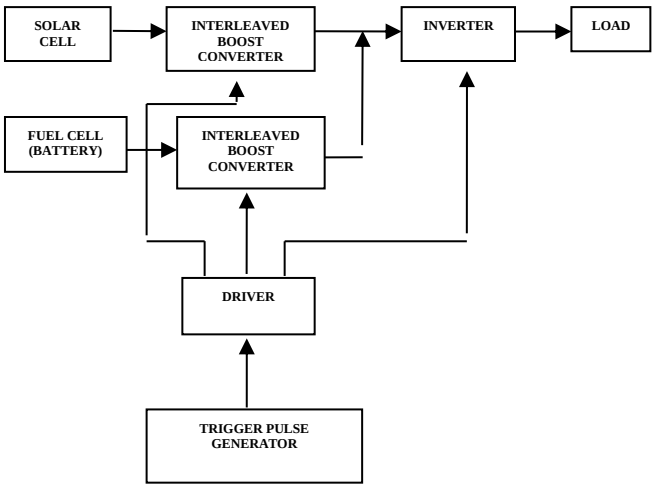

Figure 1: Hybrid system with multi-connected interleaved boost converter

III. ANALYSIS OF PROPOSED CIRCUIT

1. Solar photo voltaic array

A group of connected photovoltaic modules, which are composed of several interconnected solar cells, is called a photovoltaic array. Most PV arrays require an inverter to convert the DC electricity produced by the modules into alternating current that can be linked to the existing infrastructure to power motors, lights, and other loads. The modules of a photovoltaic array are usually connected in series to obtain the necessary voltage, and the individual strings are then connected in parallel to boost the output of current[9].

A group of connected photovoltaic modules, which are composed of several interconnected solar cells, is called a photovoltaic array. Through the photovoltaic effect, the cells transform solar energy into direct current electricity. To transform the DC electricity generated by the modules into alternating current that can be connected to the current infrastructure to power lights, motors, and other loads, the majority of PV arrays require an inverter. Typically, a PV array's modules are connected in series to get the required voltage, and then the individual strings are connected in parallel to increase the system's current output.

2. Characteristics of PV solar panel

Figure 2 depicts a PV module's comparable circuit. Figure 3 dis cal output characteristics, and equation (2.1) he characteristic equation for this PV model.

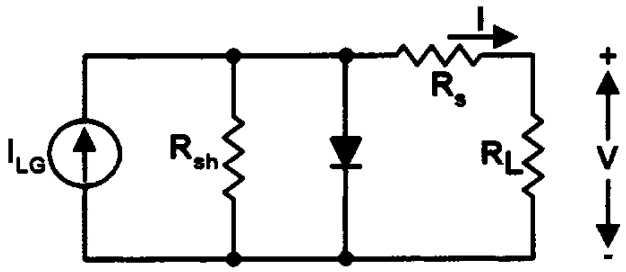

Figure 2: Equivalent circuit of a PV module

$$I = I_{LG} - I_{or}\{\exp[\frac{q}{AKT}(V + IR_s)] - 1\} - \frac{V + IR_s}{R_{sh}}$$

Where,

$$I_{or} = I_{or}\left[\frac{T}{T_{or}}\right]^3 \exp\left[\frac{qE_{go}}{Bk}\left(\frac{1}{T_r} - \frac{1}{T}\right)\right]$$

$$I_{LG} = [I_{SCR} + K_I(T - 25^\circ)]\lambda / 100$$

I	Cell output current;
V	Cell output voltage;
I_{os}	Cell reverse saturation current;
T	Cell temperature in ^{o}c;
K	Boltzmann's constant;
q	Electronic charge;
$k_I = 0.0017$	Short circuit temperature coefficient;
λ	Solar irradiation in W/m^2 ;
I_{SCR}	Short-circuit current at 25^{o} C;
I_{LG}	Light-generated current;
EGO	Band gap for silicon;
B=A=1.92	Ideality factors;
T_r=301.18^{o}k	Reference temperature;
I_{or}	Cell saturation current at T_r ;
R_{sh}	Shunt resistance;
R_s	Series resistance.

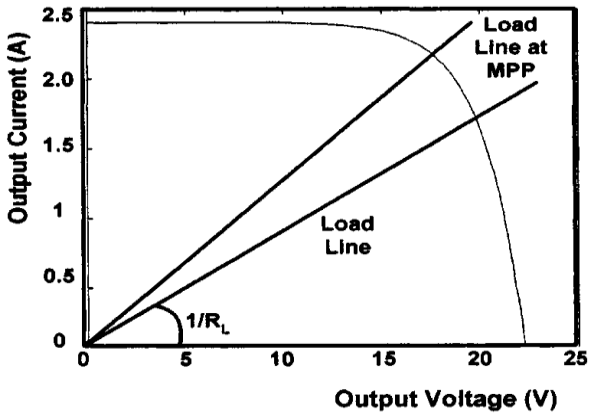

Figure 3: Current - voltage characteristics

The PV output voltage is primarily impacted by temperature fluctuations. However, the PV output current is mostly impacted by changes in irradiance. The operational point is determined by the point where the load-line and the PV module's I-V characteristic connect at a specific temperature and irradiance. The load-line adjustment under different air conditions determines the maximum power production.

3. Fuel cell

Figure 4 depicts the proton exchange membrane (PEM) fuel cell. Its electrolyte is a thin, permeable polymeric membrane. The membrane is light and tiny. Platinum electrodes are positioned on either side of the membrane to catalyze the process[10]. Hydrogen molecules are delivered to the anode of the PEM fuel cell unit, where they split into hydrogen protons and electrons. To generate electricity, the electrons are forced around an external circuit while the protons go across the polymeric membrane to the cathode. The cathode receives oxygen (in the form of air), which reacts with the hydrogen ions to create water.

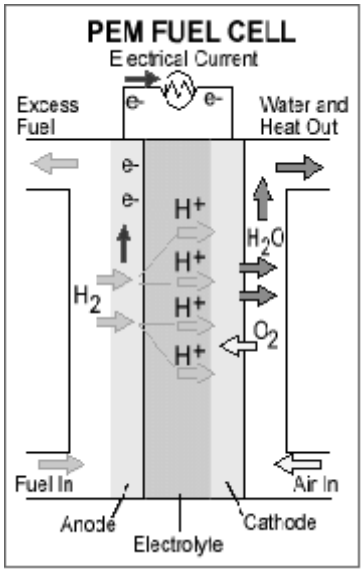

Figure 4: Fuel cell

Chemical Equation:
Anode : $2H_2 = 4H^+ + 4e^-$
Cathode: $O_2 + 4H^+ + 4e^- = 2H_2O$

Since each cell generates about 1.1 volts, stacks are created by combining the cells to achieve the necessary voltage. Bipolar plates that separate each cell serve as a pathway for the distribution of hydrogen fuel and a means of current extraction. PEM fuel cells are regarded to have the best energy density of all the fuel cells and, due to the nature of the reaction, the quickest start-up time (less than 1 second), which makes them the favored choice for applications such as backup power, portable power, and car settings. High temperature membranes that function at 150°C have been developed as a result of the catalysts' sensitivity for contaminants like carbon monoxide.

H***ydrogen***

Through channels in flow field plates, hydrogen travels to the anode, where it is separated into protons and electrons by the platinum catalyst. Direct hydrogen supply to a fuel cell is also an option, as is obtaining hydrogen from petroleum, methanol, or natural gas using a fuel processor that catalyzes a chemical reaction to produce hydrogen and carbon dioxide.

Membrane electrode assembly

Anode and cathode electrodes with a very thin coating of catalyst attached to both sides of a proton exchange membrane make up each membrane electrode assembly.
Air

Air travels to the cathode via the channels in flow field plates. Pure water and heat are created when the hydrogen protons that pass through the proton exchange membrane mix with airborne oxygen and electrons that have returned from the external circuit. The water produced as a byproduct of the electrochemical process is likewise eliminated by the air stream.

Flow field plates and stack

Through channels made in flow field plates, gases (air and hydrogen) are delivered to the electrodes of the membrane electrode assembly. A fuel cell stack is created by combining separate fuel cells to produce the required quantity of electrical power. While raising the surface area of the cells improves the current, increasing the number of cells in a stack raises the voltage.

4. Inter leaved boost converter

It transforms a low-voltage DC supply into a high-voltage one. The MOSFET's firing angle is regulated to regulate the output voltage. The output ripple current is decreased by using an interleaved concetpt.
Two MOSFETs, inductance, a DC supply, and a load make up this device. All MOSFETs receive the external triggering pulse. Equal current sharing between the parallel converters is ensured when the DC source is connected to the converter. The purpose of this converter is to lower output ripple and boost output power. The voltage measurement is used to determine the output voltage. The load is connected to the interleaved boost converter's output.

Circuit configuration

The suggested interleaved boost converter module is seen in Figure 5. One step-up conversion unit is made up of inductor L1, MOSFET active switch S1, and diode D1, while the other is made up of the parts with the subscript "2." The inherent anti-parallel diode and output capacitance of MOSFET Sx are denoted by Dsx and Csx, respectively. The output capacitor Co and the load are refilled by the voltage source Vin through the two paralleled converters.

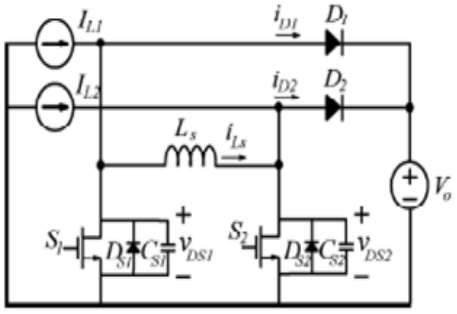

Figure 5: Simplified circuit diagram

In order to achieve zero-voltage turn ON (ZVS) and increase converter efficiency, inductor LS is switched with two active MOSFET switches to release the electric charge held in the output capacitor Csx before Sx turns ON. Current and voltage sources are used in place of L1, L2, and C0 to make the analysis simpler[11,12].

.

Circuit operation analysis

Prior to circuit analysis, the following presumptions are made.
1) The output voltage ripple can be reasonably ignored due to the size of the output capacitor C0.
2) MOSFET S1, S2, and diodes D1 and D2 forward voltage drops are disregarded.

3) Inductors L1 and L2 have similar constant currents (IL1=IL2=IL) and a huge inductance.
4) Switches CS1 and CS2 have identical output capacitances, so that CS1=CS2=CS.
Pulse width-modulation (PWM) control signals are used to operate the two active switches, S1 and S2. They have the same duty ratios and frequencies when gated. For half a switching cycle, the rising edges of the two gating signals are kept apart.
There are eight modes in which the converter operates.

.

A.Mode-1 { $t_0 < t < t_1$ }

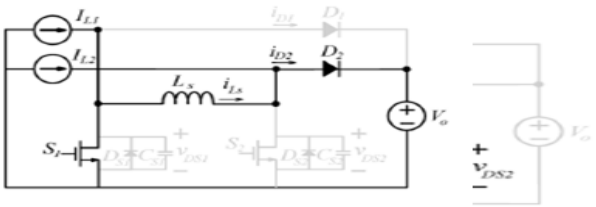

Figure 5(a)

The voltage VDS2 increases to V0 at t0 prior to this mode, and the gating signal for switch S2 has already sent to low state. Current passing through S2 fully commutates to D2 to supply the load at the start of this mode. As IL1 passes through LS, current IS1 returns from a negative value near zero. The voltage across inductor LS is V0 because of the zero voltage on VDS; thus, iLS will fall linearly at the rate of V0/LS. The current passing through S1 increases linearly in the meantime.
While iD2 = IL2, when iLS falls to zero, current is1 only contains IL1. Together with IL1, current iLS will flow through S1 in the opposite direction.iD2 continuously drops to zero while iLS rises in a negative direction. This mode ends when iLS = -IL2, which causes diode D2 to turn off. Even though iS1 and ILS currents differ slightly from zero and IL1 currents iLS, is1, iD2, and the duration of this mode t01, they can be roughly estimated as

$$i_{Ls}(t) = I_L - \frac{V_o}{L_S}t$$
$$i_{S1}(t) = \frac{V_o}{L_S}t$$
$$i_{D2}(t) = 2I_L - \frac{V_o}{L_S}t$$
$$t_{01} = \left(\frac{3}{4} - D_{\text{eff}}\right)T_S - \frac{\sin^{-1}(V_o/(V_o + 2I_L/\omega C_S))}{\omega}$$

where D_{eff} is the effective duty ratio
$\omega = 1/\sqrt{L_S C_S}$.

B. Mode II { $t_1 < t < t_2$ }

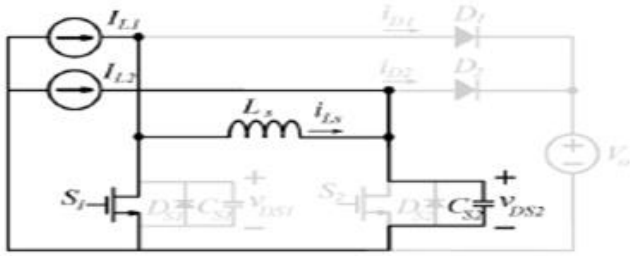

Figure 5(b)

The capacitor CS2 is no longer clamped at V0, but diode D2 ceases to conduct. As the current via LS and iLS keeps rising, it starts to release CS2. When the voltage across switch S2, vDS2, falls to zero, this mode will end. Current iLS and voltage vDS2 are equivalent as

$$v_{DS2}(t) = V_o \cos(\omega t)$$
$$i_{Ls}(t) = -V_o \omega C_S \sin(\omega t) - I_L$$
$$t_{12} = \frac{\pi}{2\omega}.$$

C. Mode III { $t_2 < t < t_3$ }

S2's anti-parallel diode, DS2, starts to conduct electricity. Through S1 and DS2, the negative directional inductor current (iLS) freewheels and maintains a value that is slightly greater than IL but equal to iLS2(t2). In this mode, switch S2's voltage is clamped to zero, making it sufficient to gate S2 at zerovoltage to turn ON.

$$t_{23} = \left(D_{\text{eff}} - \frac{1}{2}\right)T_S. \qquad (8)$$

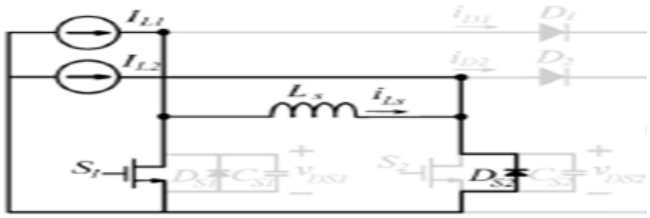

Figure 5(c)

D. Mode IV { $t_3 < t < t_4$ }

At t=t3, the switch S1 becomes inactive. The capacitor CS1 starts to be charged by current iLS. IL1 and iLS are included in the charging current. iLS slightly drops and resonates toward -IL2 as a result of the capacitor CS1 recovering a small amount of electric charge. In actuality, even with a somewhat larger magnitude, iLS will not equal -IL2 at t4. But if the small difference is ignored, the voltage on switch S1 and the current flowing through LS can be roughly calculated as

$$v_{DS1}(t) = \left(V_o + \frac{2I_L}{\omega C_S}\right)\sin(\omega t) \quad (9)$$

$$i_{Ls}(t) = I_L - (V_o \omega C_S + 2I_L)\cos(\omega t) \quad (10)$$

$$t_{34} = \frac{\sin^{-1}\left(V_o/(V_o + 2I_L/\omega C_S)\right)}{\omega}. \quad (11)$$

This mode will terminate because D1 will be forward-biased as the capacitor voltage vCS1 climbs to V0. The situation where switch S2 goes from an OFF state to ZVS to ON is described by modes I–IV. The corresponding operations from modes V–VIII for switch S1 will be identical to those from S2.

.

Inverter

As seen in figure 6, an inverter is an electrical device that changes direct current (DC) into alternating current (AC).

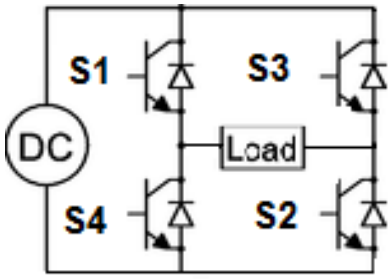

Figure 6: Inverter circuit diagram

The two modes of operation that are involved are

Mode 1: (0˚ to 180˚)

Switches S1 and S2 are activated in this mode, resulting in the output AC voltage waveform's positive half cycle.

.

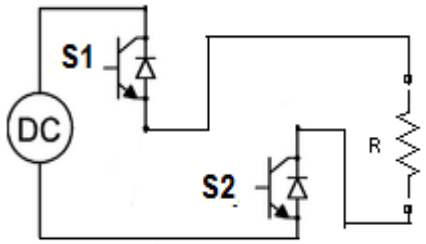

Figure 6(a)

Mode 2: (180˚ to 360˚)

During this mode, switches S3 and S4 is turned ON which yields to the negative half cycle of the output AC voltage waveform.

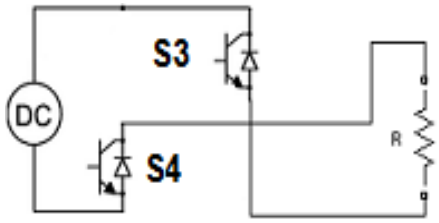

Figure 6(b)

IV DESIGN OF L,C AND D VALUES

Input voltage (Vs) = 15V
Output voltage (V_o) = 57V
Ripple current (ΔI) = 0.9A
Ripple voltage (ΔV_c) = 100mV
Switching frequency (Fs) = 65 KHz
The L, C, D values are designed using following formulae

$$D = 1 - \frac{V_s}{V_o} \quad (3.1)$$

$$L = \frac{V_s * D}{\Delta I * F_s} \quad (3.2)$$

$$c = \frac{I_a * D}{\Delta V_c * F_s} \quad (3.3)$$

After substituting all the values in the equation,

D = 0.5
L = 200mH
C = 1200µF

V SIMULATION CIRCUIT AND RESULT

The interleaved boost converter simulation circuit diagram is displayed in the figure below. MOSFET switches, designated M1, M2, M3, M4, M5, and M6, are employed in this circuit. The dc supply for the input is provided. MATLAB's scope block is used to inspect the output AC supply.

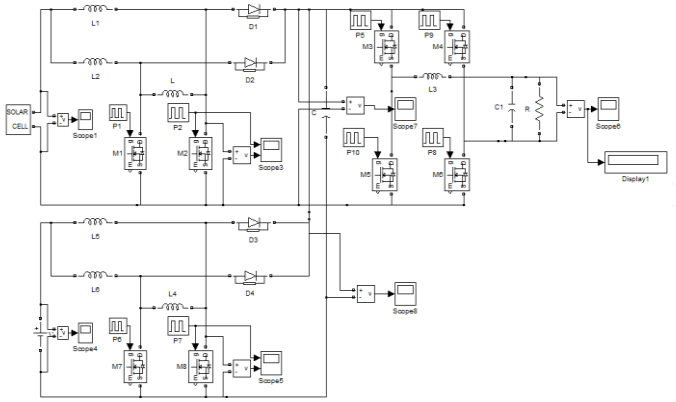

Figure 7: Simulation circuit diagram

The input solar cell source of magnitude 15V is shown in Figure 7.1. The interleaved boost converter receives this voltage and uses it to increase the input source voltage.

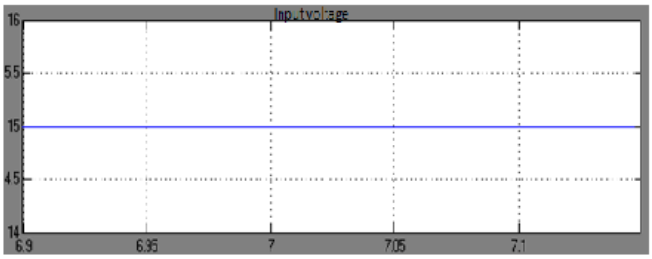

Figure 7.1: Solar cell voltage waveform

The input battery cell source of magnitude 15V is shown in Figure 7.2. The interleaved boost converter receives this voltage and uses it to increase the input source voltage.

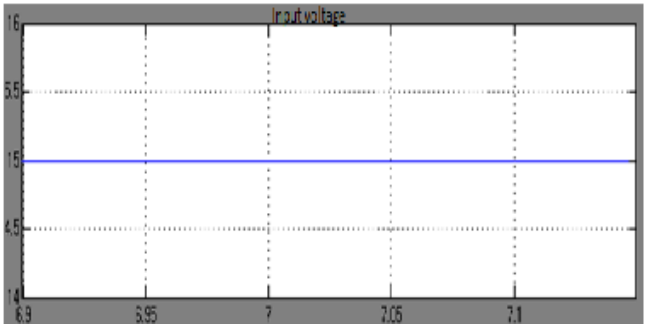

Figure 7.2: Battery voltage waveform

The MOSFET switching pulses for switches M1 and M2 are shown in Figure 7.3. First, a gate pulse is applied to turn on the M2 switch. After a little delay, the M2 switch is in the on state. The pulse generator produces these pulses.

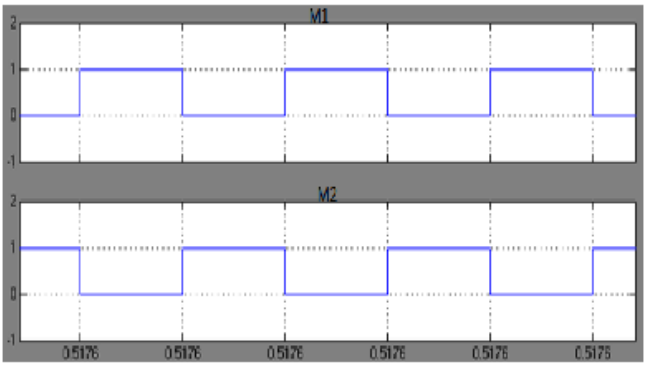

Figure 7.3: Switching pulse of M1 and M2

The voltage across the gate and the voltage between the drain and the source are shown in Figure 7.4. The output waveform is displayed below if the gate pulse voltage is applied to the gate terminal.

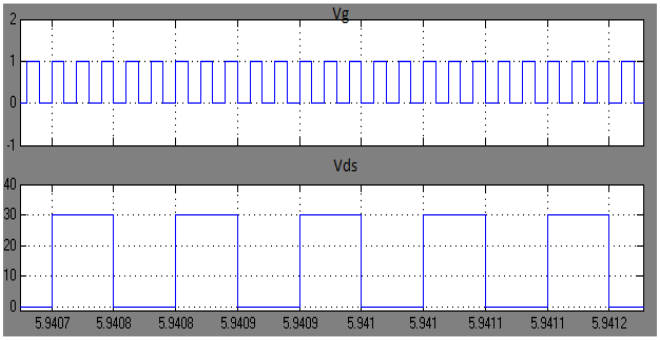

Figure 7.4:Vg and Vds waveform

The features of interleaved boost converter operation are shown in Figure 7.5. The suggested converter is supplied with a frequency of 65 kHz and an input voltage of 15V. 55V is the maximum output voltage.

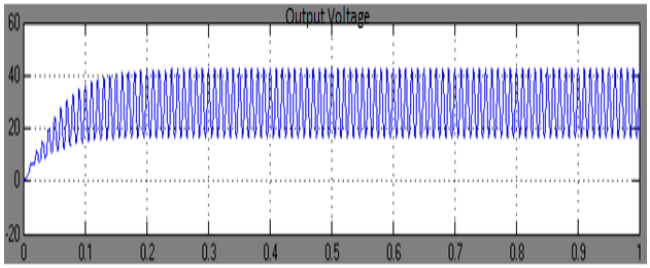

Figure 7.5:Output voltage of interleaved boost converter

The output voltage waveform of the inverter that transforms a constant 55V dc source into an ac voltage is shown in Figure 7.6. The suggested converter's output waveform is displayed together with the input voltage of 15V.

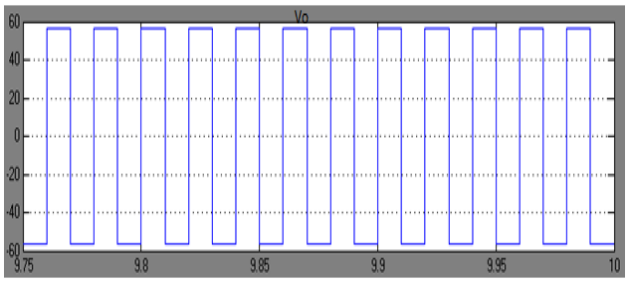

Figure 7.6: Output voltage waveform

V CONCLUSION

Using Matlab Simulink software, the module layout simulation was successfully completed, and the resulting waveforms were examined. Analysis is done on the interleaved boost converter's output replies. The MPPT control algorithm can be used to maximize the PV array output power delivered to a load. Future developments will be greatly impacted by the creation of affordable power conversion devices for PV energy. A solar panel's output voltage must be converted into usable dc or ac voltage at its greatest power point.

REFERENCE

1. Kumar, G. Kiran, and G. Arunkumar. "Multiple input interleaved boost converter for non-conventional energy applications." In *2019 Innovations in Power and Advanced Computing Technologies (i-PACT)*, vol. 1, pp. 1-5. IEEE, 2019.
2. Zheng, Yifei, Wenhao Xie, and Keyue Ma Smedley. "Interleaved high step-up converter with coupled inductors." *IEEE Transactions on Power Electronics* 34, no. 7 (2018): 6478-6488.
3. Xian, Liang, and Youyi Wang. "Exact steady-state analysis in multiple-input converters applied with diverse time-sharing switching schemes." *IET Power Electronics* 8, no. 5 (2015): 724-734.
4. Quan, Zhongyi, Yun Wei Li, and Changpeng Jiang. "Design of interleaved converters with minimum filtering requirement." In *2019 IEEE Applied Power Electronics Conference and Exposition (APEC)*, pp. 404-411. IEEE, 2019.
5. Choung, Seung H., and Alexis Kwasinski. "Multiple-input DC-DC converter topologies comparison." In *2008 34th Annual Conference of IEEE Industrial Electronics*, pp. 2359-2364. IEEE, 2008.
6. Smith, Nadia, and Roy McCann. "Investigation of a multiple input converter for grid connected thermoelectric-photovoltaic hybrid system." In *2012 IEEE Green Technologies Conference*, pp. 1-5. IEEE, 2012.
7. Han, Jungho, and Joong-Ho Song. "Phase current-balance control using DC-link current sensor for multiphase converters with discontinuous current mode considered." *IEEE Transactions on Industrial Electronics* 63, no. 7 (2016): 4020-4030.
8. Y. K. Semero, D. Zheng, and J. Zhang, “A PSO-ANFIS based hybrid approach for short term PV power prediction in microgrids,” Electr. Power Components Syst., vol. 46, no. 1, pp. 95–103, 2018.
9. Filsoof, Kia, and Peter W. Lehn. "A bidirectional multiple-input multiple-output modular multilevel DC–DC converter and its control design." *IEEE Transactions on Power Electronics* 31, no. 4 (2015): 2767-2779.
10. Bae, Sungwoo, and Alexis Kwasinski. "Maximum power point tracker for a multiple-input Ćuk dc-dc converter." In *INTELEC 2009-31st International Telecommunications Energy Conference*, pp. 1-5. IEEE, 2009.
11. Liu, Yuan-Chuan, and Yaow-Ming Chen. "A systematic approach to synthesizing multi-input DC–DC converters." *IEEE Transactions on Power Electronics* 24, no. 1 (2009): 116-127.
12. Smith, Nadia, and Roy McCann. "Analysis and simulation of a multiple input interleaved boost converter for renewable energy applications." In *2014 IEEE 36th International Telecommunications Energy Conference (INTELEC)*, pp. 1-7. IEEE, 2014.